Supporting Information

A strategy of chiral cation coordination to achieve a large luminescence dissymmetry factor in 1D hybrid manganese halides

Fei Wang,[abc] Xingjun Li,*[abc,] Tianqi Chen,[abc] Liqing Wang,[ac] Chenliang Li,[ac] Wei Zhang,[ac] Wen Yuan,[abc] Shan Lu,[abc] Lina Li,[abc] and Xueyuan Chen[abc]

[a]State Key Laboratory of Structural Chemistry, and Fujian Key Laboratory of Nanomaterials, Fujian Institute of Research on the Structure of Matter, Chinese Academy of Sciences, Fuzhou, Fujian 350002, China.
[b]College of Chemistry and Materials Science, Fujian Normal University, Fuzhou, Fujian 350117, China.
[c]Fujian College, University of Chinese Academy of Sciences, Fuzhou, Fujian 350116, China.
* Corresponding author, E-mail: lixj@fjirsm.ac.cn

1. Materials and Instrumentation

Materials

Manganese acetate ($Mn(CH_3COO)_2$, 99%), (1*R,* 2*R*)-2-aminocyclohexanol (*RR*-DACA, 98%), (1*S*, 2*S*)-2-aminocyclohexanol (*SS*-DACA, 98%), hydrobromic acid (HBr, 48%) were purchased from Aladdin (Shanghai, China). Diethyl ether ($C_4H_{10}O$, 98%) was sourced from Sinopharm Chemical Reagent Co., Ltd. All reagents were employed as received without post-synthesis treatment.

Instrumentation

Single-crystal X-ray diffraction (SCXRD) data of *R/S*-$DACAMnBr_3$ were collected using Bruker D8 Advance equipped with Mo-Kα (λ = 0.71073 Å) radiation at 100 K. Powder X-ray diffraction (PXRD) patterns were conducted on an X-ray diffractometer (MiniFlex 600, Rigaku) with Cu Kα1 radiation (λ = 1.54187 Å). X-ray photoelectron spectra (XPS) were performed on a Thermo Fisher ESCALAB 250 Xi X-ray photoelectron spectroscopy with Al Kα (15 kV, 20 mA) as the sources of radiation. Fourier transform infrared (FT-IR) spectra were measured in a Magna 750 FTIR spectrometer from samples in KBr pellets. Thermogravimetric analysis (TGA) was tested on a thermal analysis system (STA449-F5 Jupiter, Netzsch, Germany) under a N_2 flow with a heating rate of 10 °C min^{-1}. The ultraviolet-visible (UV-Vis) absorption spectra were detected by the spectrometer PerkinElmer Lambda 950. Photoluminescence excitation (PLE) and photoluminescence (PL) emission spectra, PL decays, absolute PL quantum yields (PLQY), and low-temperature measurements were measured on the FLS980 spectrometer (Edinburgh) equipped with both a continuous (450 W), pulsed flash lamp, an OPO nanosecond pulsed laser and a THMS 600 temperature-variable stage. PL photos were taken by an iPhone 14 cell phone without any filter. The CPL spectra of the samples were measured on a JASCO CPL-300 spectrometer (λ_{ex} = 357 nm) and the collection wavelength was around 626 nm. The circular dichroism (CD) spectra were collected on a J-1500 CD spectrometer with a KBr pellet as a background. The electron paramagnetic resonance (EPR) spectrum was collected on a JES-FA200 spectrometer (HITACHI) at room temperature.

The crystallographic data supporting this paper can be obtained for free from the Cambridge Crystallographic Data Centre (CCDC) under the accession numbers 2378510 and 2378511 at https://www.ccdc.cam.ac.uk/data_request/cif.

2. Experimental Procedures

Synthesis of *R/S*-DACAMnBr$_3$ crystals

R-DACAMnBr$_3$ crystals were synthesized via supersaturated recrystallization. Typically, a homogeneous solution was obtained by dissolving 3 mmol Mn(CH$_3$COO)$_2$ in 3 mL HBr within a 50 mL flask, followed by constant stirring at 125 °C for 60 min under ambient conditions. Subsequently, 3 mmol of *RR/SS*-DACA was added to the mixed solution under continuous stirring for 60 min. Light pink crystals of *R*-DACAMnBr$_3$ were produced by gradual cooling to RT naturally. Finally, the crystals were washed five times with diethyl ether and dried at 75 ℃ for 1h. The *S*-DACAMnBr$_3$ crystals were prepared via the same synthetic procedure of *R*-DACAMnBr$_3$ crystals, except that *RR*-DACA was replaced by *SS*-DACA.

Fabrication and measurements of CP-LEDs

CP-LEDs were constructed by coupling *R/S*-DACAMnBr$_3$ crystals to a commercially available ultraviolet (UV) chip (λ_{em} = 365 nm, 3 V). *R/S*-DACAMnBr$_3$ powders were homogenously blended with UV-curable adhesive and subsequently applied onto the chip surface. The encapsulated devices were further cured under 365 nm UV light for 15 min, and assembled into a portable lamp colorimeter system for operational configuration. The spectral emission profiles and optoelectronic performance of the CP-LEDs were measured by using a HAAS2000 spectroradiometer equipped with a temperature-regulated integrating sphere apparatus.

Fabrication and measurements of photodetectors

Photoelectric measurements were performed with planar electrodes. Two symmetric Ag electrodes were deposited on the both ends of a single *R/S*-DACAMnBr$_3$ crystal, and the channel between neighboring electrodes has areas of 0.01 cm^2. The current-voltage (I-V) and current-time curves (I-t) were measured by using a high-precision electrometer (Keithley 6517B).

Table S1. Crystal structure parameters of *R/S*-DACAMnBr$_3$.

Name	*R*-DACAMnBr$_3$	*S*-DACAMnBr$_3$
Identification code	*R*-DACAMnBr$_3$_auto	*S*-DACAMnBr$_3$_auto
Empirical formula	$C_6H_{14}NOMnBr_3$	$C_6H_{14}NOMnBr_3$
Formula weight	410.85	410.85
Temperature/K	99.99(10)	100.00(10)
Crystal system	orthorhombic	orthorhombic
Space group	$P2_12_12_1$	$P2_12_12_1$
a/Å	7.7707(3)	7.7824(4)
b/Å	8.0410(3)	8.0325(4)
c/Å	19.5459(7)	19.5413(8)
α/°	90	90
β/°	90	90
γ/°	90	90
Volume/Å^3	1221.31(11)	1221.57(10)
Z	4	4
ρ_{calc} g/cm^3	2.234	2.234
μ/mm^{-1}	10.857	10.855
F(000)	780.0	780.0
Crystal size/mm^3	0.15 × 0.45 × 0.10	0.15 × 0.45 × 0.10
Radiation	Mo Kα (λ = 0.71073)	Mo Kα (λ = 0.71073)
2θ range for data collection/°	4.168 to 61.458	4.168 to 61.306
Index ranges	-9 ≤ h ≤ 10，-11 ≤ k ≤ 9，-25 ≤ l ≤ 28	-8 ≤ h ≤ 11，-10 ≤ k ≤ 7，-26 ≤ l ≤ 20
Reflections collected	7462	6217
Independent reflections	2989 [R_{int} = 0.0239, R_{sigma} = 0.0346]	2775 [R_{int} = 0.0367, R_{sigma} = 0.0510]
Data/restraints/parameters	2989/3/114	2775/0/114
Goodness-of-fit on F^2	1.002	1.045
Final R indexes [I>=2σ (I)]	R_1 = 0.0215, wR_2 = 0.0401	R_1 = 0.0329, wR_2 = 0.0711
Final R indexes [all data]	R_1 = 0.0275, wR_2= 0.0410	R_1 = 0.0394, wR_2= 0.0737
Flack parameter	-0.010(9)	0.013(12)
CCDC	2378510	2378511

$R_1 = \sum||F_o|-|F_c||/\sum|F_o|$. $wR_2 = [\sum w(F_o^2-F_c^2)^2/\sum w(F_o^2)^2]^{1/2}$

Table S2. Bond lengths (Å) of *R*-DACAMnBr$_3$.

Bond lengths (Å)			
Br1-Mn1[1]	2.6963(7)	N1-C2	1.505(5)
Br1-Mn1	2.7031(7)	C2-C1	1.522(5)
Br2-Mn1	2.7112(7)	C2-C3	1.524(5)
Br2-Mn1[1]	2.7076(7)	C1-C6	1.513(6)
Br3-Mn1	2.6708(7)	C5-C4	1.526(6)
Mn1-O1	2.218(3)	C5-C6	1.533(6)
O1-C1	1.452(4)	C4-C3	1.530(6)

Table S3. Bond lengths (Å) of *S*-DACAMnBr$_3$.

Bond lengths (Å)			
Br01-Mn1	2.6993(13)	C1-C2	1.501(11)
Br01-Mn1^1	2.7040(12)	C1-C6	1.524(9)
Br02-Mn1^2	2.7092(13)	C4-C5	1.512(13)
Br02-Mn1	2.7089(13)	C4-C3	1.535(10)
Br03-Mn1	2.6691(13)	N1-C2	1.522(8)
Mn1-O1	2.223(5)	C5-C6	1.541(9)
O1-C1	1.453(7)	C2-C3	1.524(9)

Table S4. Bond angles (°) of *R*-DACAMnBr$_3$.

Bond angles (°)			
Mn1^1-Br1-Mn1	92.493(12)	O1-Mn1-Br2	86.56(7)
Mn1^1-Br2-Mn1	92.068(12)	O1-Mn1-Br2^2	86.08(7)
Br1^2-Mn1-Br1	172.80(3)	O1-Mn1-Br3	176.33(7)
Br1^2-Mn1-Br2	91.59(2)	C1-O1-Mn1	129.7(2)
Br1-Mn1-Br2^2	94.61(2)	N1-C2-C1	107.1(3)
Br1-Mn1-Br2	86.35(2)	N1-C2-C3	109.9(3)
Br2^2-Mn1-Br2^2	86.56(2)	C1-C2-C3	111.8(3)
Br2^2-Mn1-Br2	172.56(3)	O1-C1-C2	108.3(3)
Br3-Mn1-Br1	91.69(2)	O1-C1-C6	112.1(3)
Br3-Mn1-Br1^2	95.42(2)	O6-C1-C2	112.1(3)
Br3-Mn1-Br2	97.09(2)	C4-C5-C6	110.4(4)
Br3-Mn1-Br2^2	90.26(2)	C5-C4-C3	110.5(4)
O1-Mn1-Br1^2	84.15(7)	C1-C6-C5	110.1(3)
O1-Mn1-Br1	88.84(7)	C2-C3-C4	110.2(4)

Table S5. Bond angles (°) of *S*-DACAMnBr$_3$.

Bond angles (°)			
Mn1-Br01-Mn1^1	92.577(19)	O1-Mn1-Br02	86.74(13)
Mn1-Br02-Mn1^2	92.25(2)	O1-Mn1-Br02^1	85.95(13)
Br01-Mn1-Br01^2	172.87(5)	O1-Mn1-Br03	176.25(14)
Br01-Mn1-Br02	91.77(4)	C1-O1-Mn1	129.3(4)
Br01-Mn1-Br02^1	86.38(4)	O1-C1-C2	108.6(6)
Br01^2-Mn1-Br02	86.29(4)	O1-C1-C6	111.3(5)
Br01^2-Mn1-Br02^1	94.68(4)	C2-C1-C6	112.1(6)
Br02-Mn1-Br02^1	172.61(5)	C5-C4-C3	110.9(6)
Br03-Mn1-Br1^2	91.62(4)	C4-C5-C6	111.1(6)
Br03-Mn1-Br01	95.43(4)	C1-C2-N1	107.6(6)
Br03-Mn1-Br02^1	90.32(4)	C1-C2-C3	112.6(6)
Br03-Mn1-Br02	96.98(4)	N1-C2-C3	109.2(6)
O1-Mn1-Br01	83.99(12)	C1-C6-C5	109.7(6)
O1-Mn1-Br01^2	89.05(12)	C2-C3-C4	110.0(6)

Table S6. Radiative rate constants (k_r) and non-radiative rate constants (k_{nr}) of *R/S*-DACAMnBr$_3$ at RT.

Sample	PLQY (%)	τ_{eff} (ms)	τ_r (ms)	k_r (s^{-1})	k_{nr} (s^{-1})
R-DACAMnBr$_3$	32.2	0.98	3.04	3.29×10^2	6.92×10^2
S-DACAMnBr$_3$	18.7	0.72	3.85	2.26×10^2	1.13×10^3

Based on the PL lifetimes and PLQYs (Φ) of *R*-DACAMnBr$_3$ crystals at RT, the k_r and k_{nr} values were calculated by using the following equation:[1]

$$\Phi = \frac{k_r}{k_r + k_{nr}} = \frac{k_r}{k_{obs}} = \frac{\tau_{obs}}{\tau_r}$$

where τ_{obs} and τ_r represent the observed and radiative decay times, respectively.

Table S7. PLQY, effective PL lifetime (τ_{eff}), radiative decay time (τ_r), radiative rate constants (k_r) and non-radiative rate constants (k_{nr}) of *R*-DACAMnBr$_3$ crystals at different temperatures (120-300 K).

Temperature (K)	PLQY (%)	τ_{eff} (ms)	τ_r (ms)	k_r (s^{-1})	k_{nr} (s^{-1})
120	32.0	1.18	3.69	2.71×10^2	5.76×10^2
160	31.8	1.16	3.65	2.74×10^2	5.88×10^2
200	31.1	1.13	3.63	2.75×10^2	6.10×10^2
240	32.6	1.06	3.25	3.08×10^2	6.35×10^2
300	31.1	0.97	3.12	3.21×10^2	7.10×10^2

Table S8. Comparison of CPL performance for chiral Mn-based OIMHs.

	CPL Materials	Bonding type	λ_{em}(nm)	$\lvert g_{lum} \rvert$	Ref.
1	*R/S*-TBM polycrystalline	hydrogen bond	519	2.5×10^{-2}	2
2	(*L*)-(tert-butyl prolinate) $MnCl_3$	hydrogen bond	646	6.3×10^{-3}	3
3	(*R*-XH^+)$_2MnBr_4$ polycrystalline	hydrogen bond	520	8.2×10^{-3}	4
4	*S*-(3-methyl piperidine) $MnCl_3$ SC	hydrogen bond	644	1.76×10^{-3}	5
5	*R*-(3-hydroxy piperidine) $MnCl_3$ SC	hydrogen bond	640	2.50×10^{-3}	5
6	(*R/S*-3-$C_4H_{12}N_2)_6(Mn_3Cl_{12})$ $(Cl)_6$ polycrystalline	hydrogen bond	630	7.1×10^{-3}	6
7	*S*-[MBA-Me_3] $MnBr_4$ SC	hydrogen bond	520	4.5×10^{-3}	7
8	(*R*-1-PPA)$_2MnBr_4$ film	hydrogen bond	510	0.01	8
9	*S*-O-H_2O polycrystalline	hydrogen bond	540	1.23×10^{-2}	9
10	*R/S*-$MnBr_3$	hydrogen bond	630	6.1×10^{-3}	10
11	*R*-$MPEA_2MnCl_4$	hydrogen bond	630	0.01	11
12	[H_2(*RR/SS*-BDPP)] $MnBr_4$ polycrystalline	hydrogen bond	523	2.0×10^{-3}	12
13	(*R*-Br-MBA)$_3MnBr_5$	hydrogen bond	634	9.1×10^{-4}	13
14	*R*-Mn (Binapo)Br_2	coordination bond	633	5.1×10^{-3}	14
15	(*R/S*-MBA) $MnCl_3 \cdot CH_3OH$ polycrystalline	coordination bond	660	1.25×10^{-2}	15
16	*SS*-1 SC	coordination bond	530	2.1×10^{-2}	16
17	*S*-[$(L)_2$MnBr] Br microcrystals	coordination bond	636	1.94×10^{-2}	17
18	$MnCl_4$-1 film	coordination bond	515	5.8×10^{-2}	18
19	(*R/S*-XH^+) $MnBr_3$ SC	coordination bond	620	0.328	4
20	*S*-DACA$MnBr_3$ SC	coordination bond	626	0.292	This work

Table S9. g_{lum} values of *R*-DACAMnBr$_3$ upon different rotation angles of the crystals.

Angle	g_{lum} (λ_{em} = 626 nm)
R-0°	-0.282
R-45°	-0.254
R-90°	-0.246
R-135°	-0.283
R-180°	-0.269
R-225°	-0.248
R-270°	-0.263
R-315°	-0.298
R-360°	-0.293
S-0°	0.292

Table S10. g_{lum} values of *R/S*-$DACAMnBr_3$ under a 1.6 T magnetic field.

Name	g_{lum}（λ_{em} = 626 nm）
R-$DACAMnBr_3$	-0.282
R-$DACAMnBr_3$-NS	-0.317
R-$DACAMnBr_3$-SN	-0.314
S-$DACAMnBr_3$	0.292
S-$DACAMnBr_3$-NS	0.317
S-$DACAMnBr_3$-SN	0.321

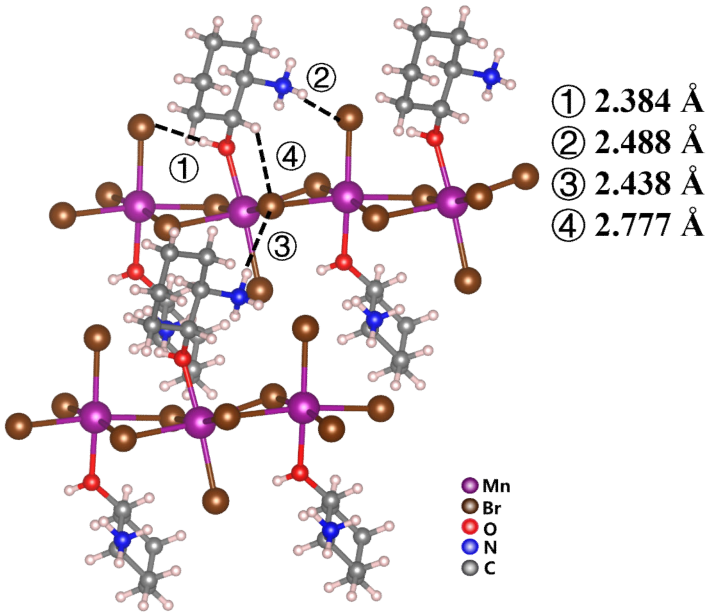

Figure S1. Schematic illustration of hydrogen bonds in *R*-DACAMnBr$_3$.

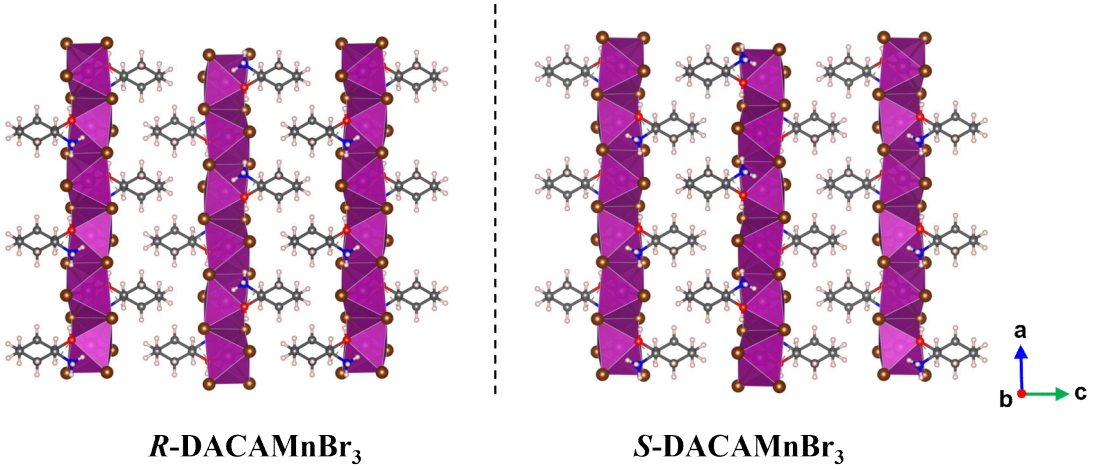

***R*-DACAMnBr$_3$** **S-DACAMnBr$_3$**

Figure S2. Packing diagram in *R/S*-DACAMnBr$_3$ showing nonsuperimposable mirror images.

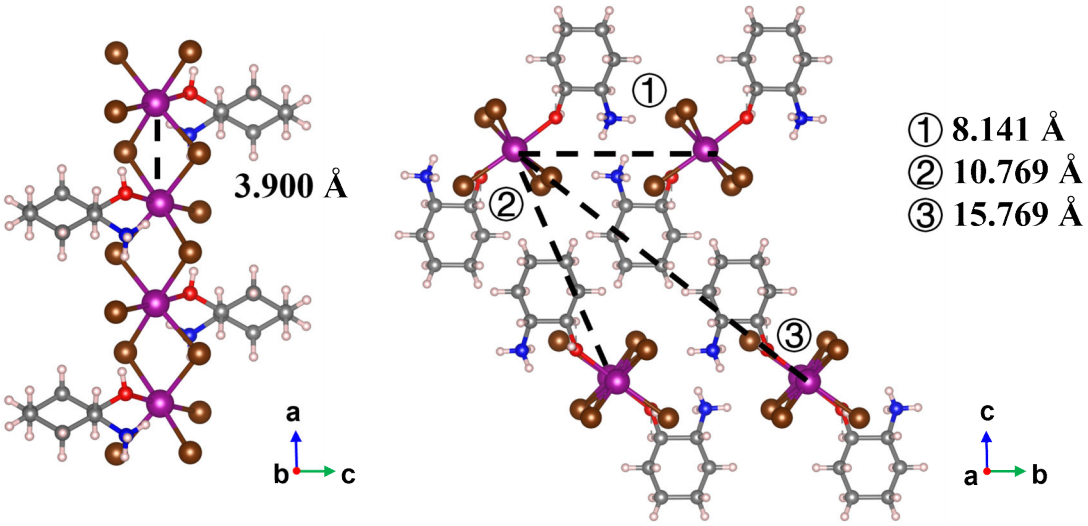

Figure S3. Crystal structure diagram showing Mn^{2+}-Mn^{2+} distance in *R*-DACAMnBr_3.

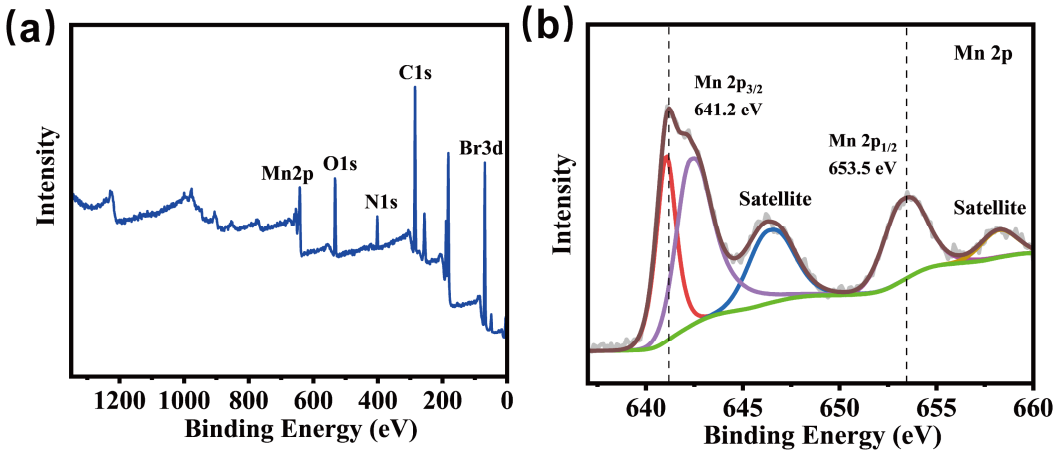

Figure S4. (a) XPS of *R*-DACAMnBr$_3$ crystals. (b) XPS energy region scan typical for Mn 2p.

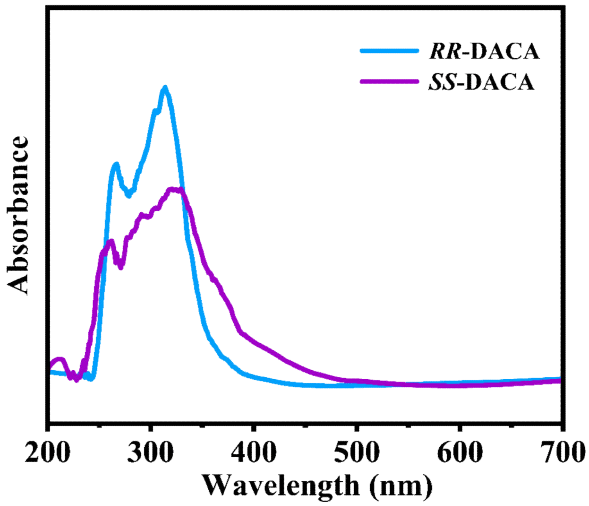

Figure S5. UV-vis absorption spectra of *RR*-DACA and *SS*-DACA ligands.

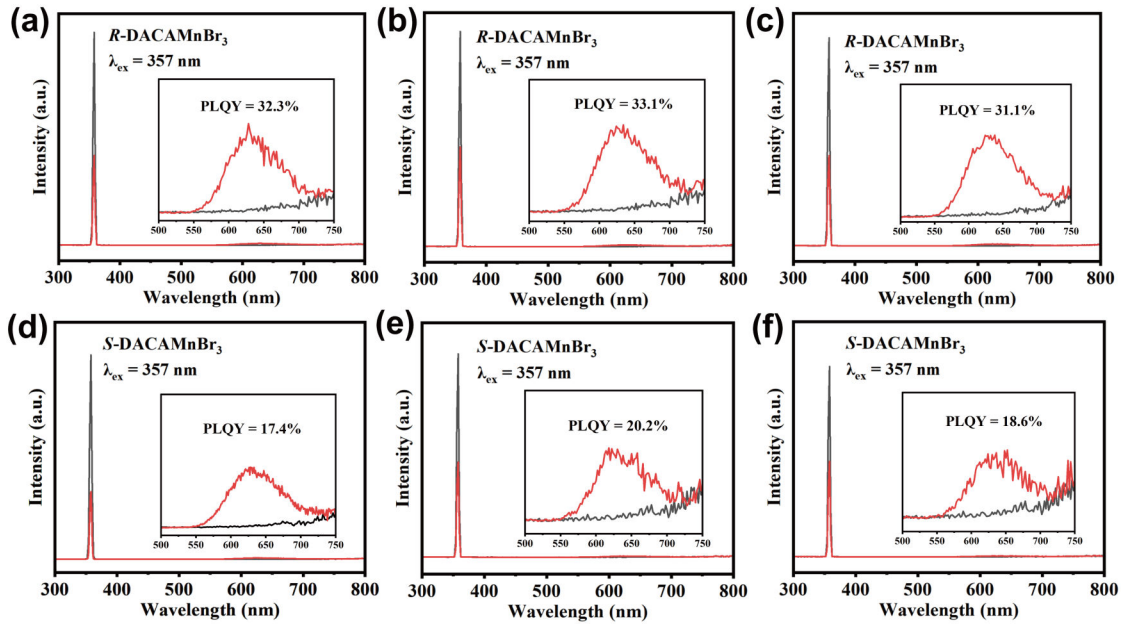

Figure S6. Determination of PLQYs for *R*/*S*-DACAMnBr$_3$ crystals (a-f). The luminescence spectra were measured independently three times to determine average PLQYs of 32.2 ± 0.8% and 18.7 ± 1.1% for *R*/*S*-DACAMnBr$_3$, respectively.

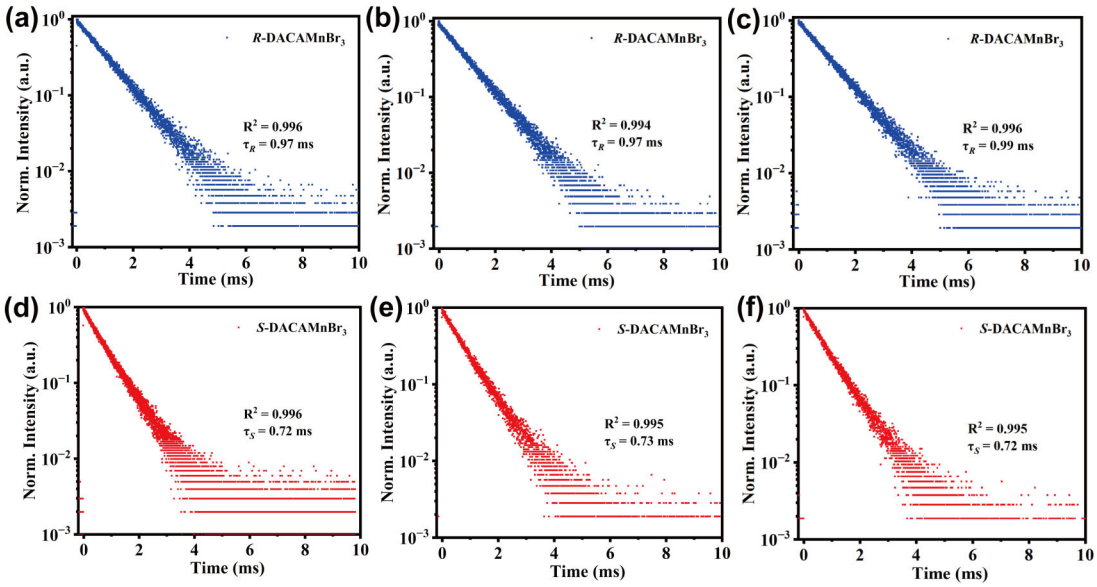

Figure S7. PL decay spectra measured from three batches of R-DACAMnBr$_3$ (a-c) and S-DACAMnBr$_3$ (d-f) crystals, showing average PL lifetimes of 0.98 and 0.72 ms for R/S-DACAMnBr3, respectively.

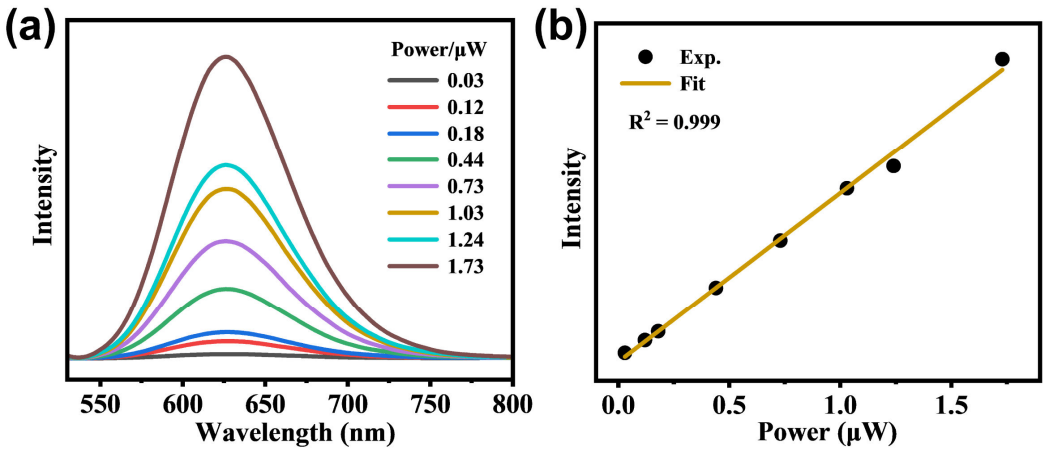

Figure S8. (a) Power-dependent PL spectra (λ_{ex} = 357 nm) of *R*-DACAMnBr$_3$ crystals. (b) Integrated PL intensities of *R*-DACAMnBr$_3$ crystals as a function of the excitation powers.

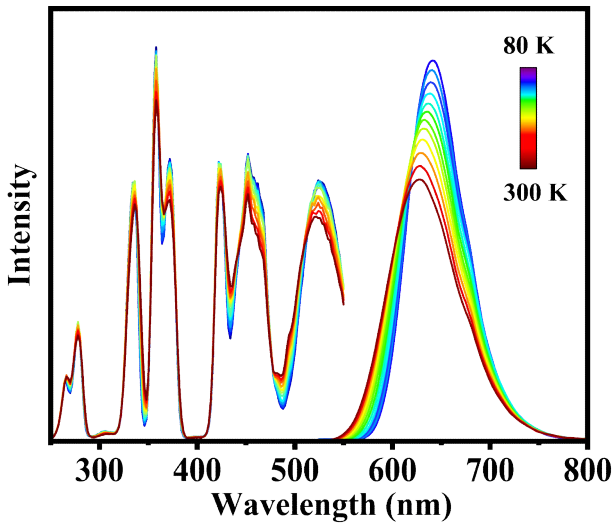

Figure S9. Temperature-dependent PL excitation (left, λ_{em} = 626 nm) and emission spectra (right, λ_{ex} =357 nm) of *R*-DACAMnBr$_3$ crystals.

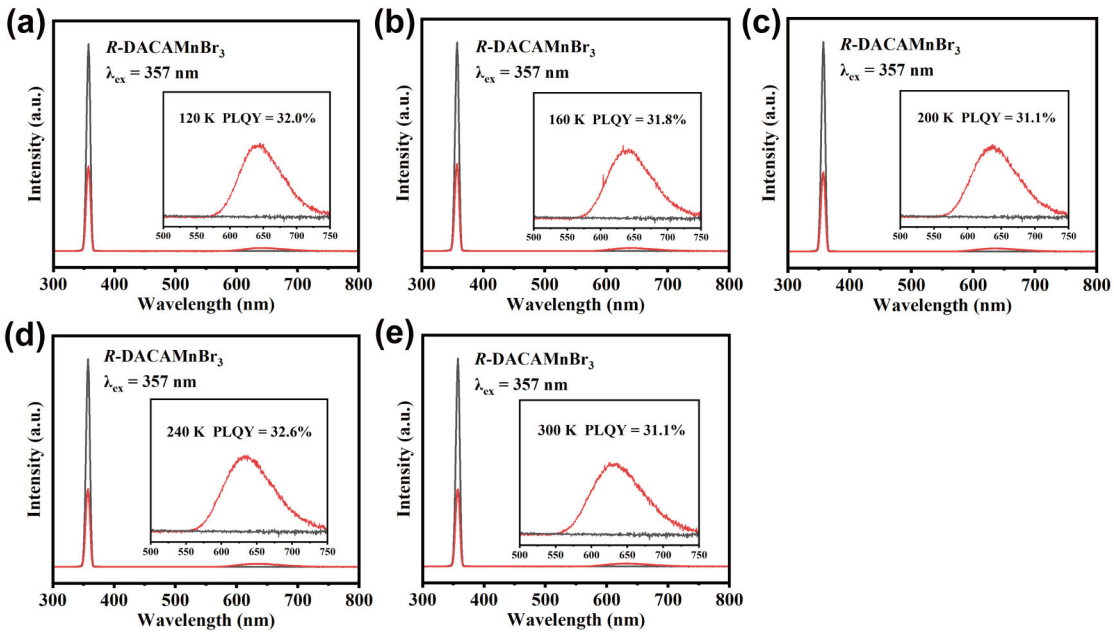

Figure S10. Determination of PLQYs for *R*-DACAMnBr$_3$ crystals at different temperatures varying from 120 to 300 K.

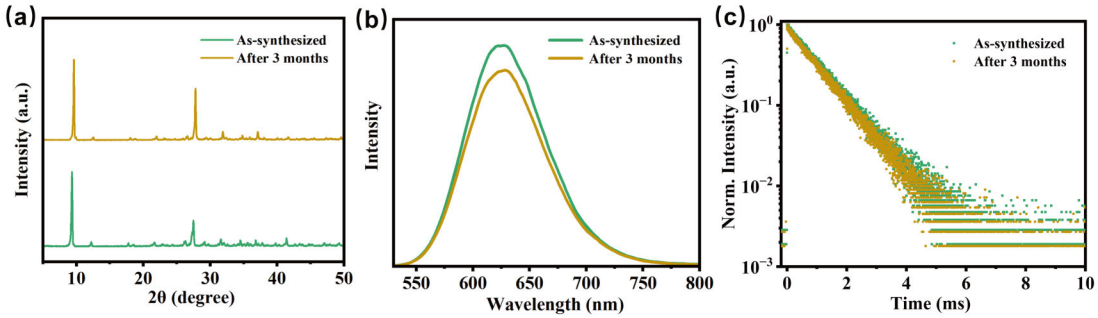

Figure S11. (a) Powder XRD patterns, (b) PL emission spectrum and (c) PL decay spectra of *R*-DACAMnBr$_3$ crystals before and after storing in a desiccator for 3 months. The XRD pattern, PL spectrum and PL lifetime of the stored crystals remained essentially unchanged, confirming the good stability of the crystals in dry air (humidity: <30%).

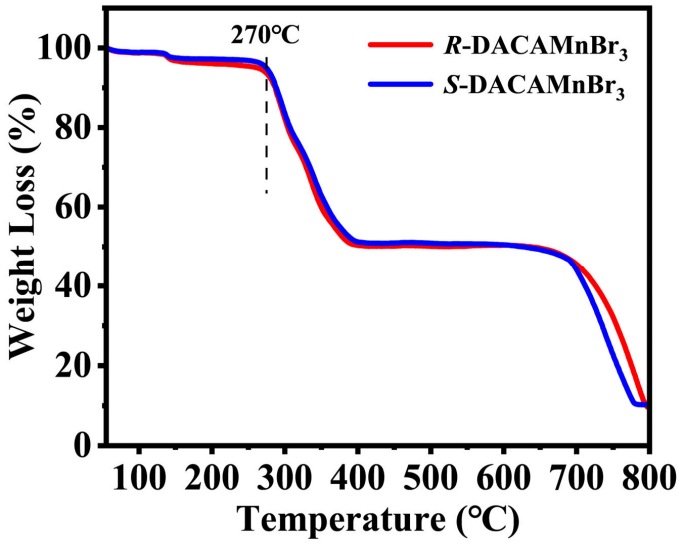

Figure S12. Thermogravimetric analysis (TGA) curves for *R/S*-DACAMnBr$_3$ crystals.

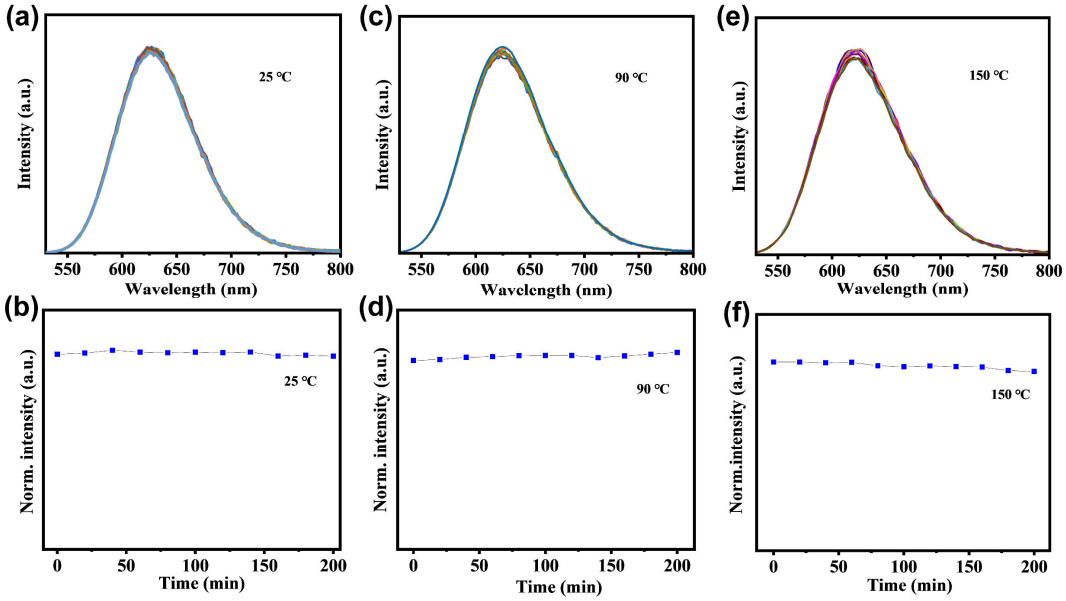

Figure S13. Time-dependent PL spectra and integrated PL intensities of *R*-DACAMnBr$_3$ crystals at (a, b) 25°C, (c, d) 90°C, and (e, f) 150°C, recorded at different time intervals under continuous illumination with a 365 nm UV lamp for 200 min.

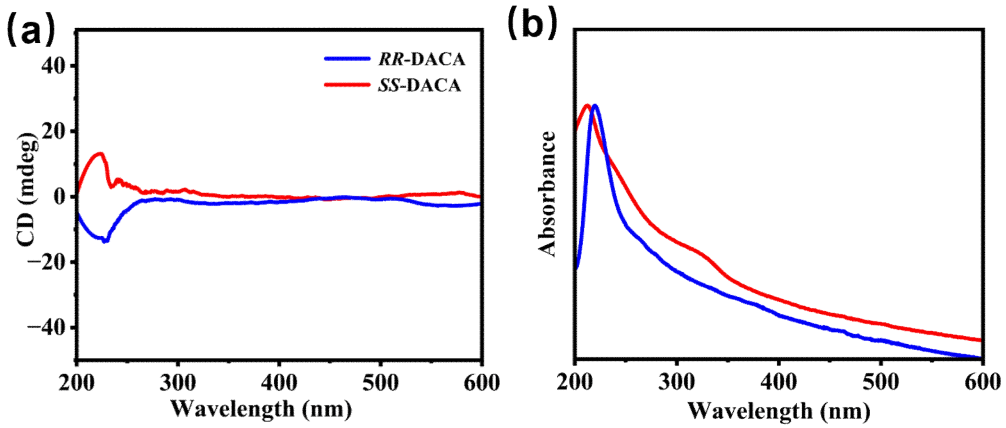

Figure S14. (a) CD and (b) UV-vis absorption spectra of *SS*-DACA and *RR*-DACA.

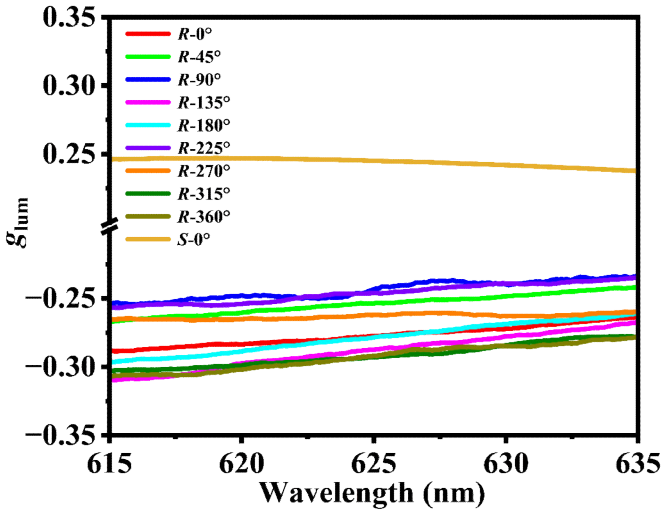

Figure S15. g_{lum} curves of *R*-DACAMnBr$_3$ single crystal with different rotation angles of the crystal.

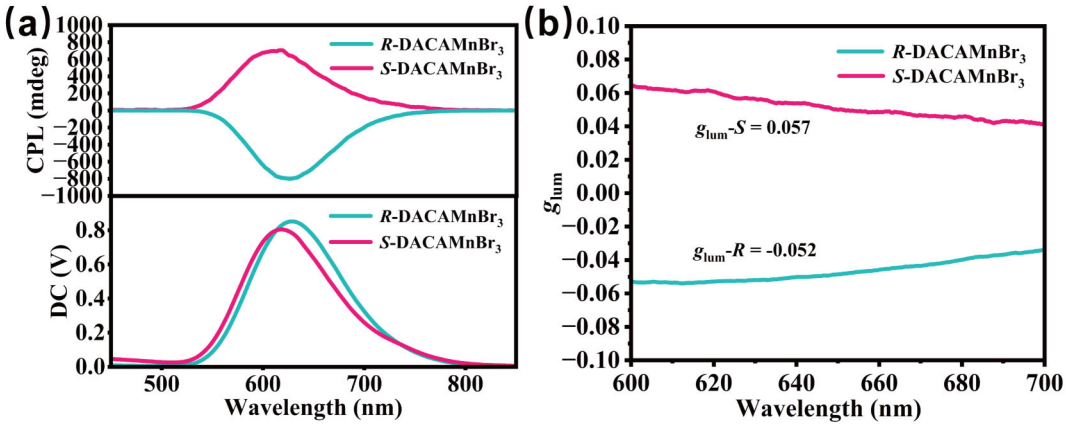

Figure S16. (a) CPL spectra and (b) g_{lum} spectra of polycrystalline *R/S*-DACAMnBr$_3$.

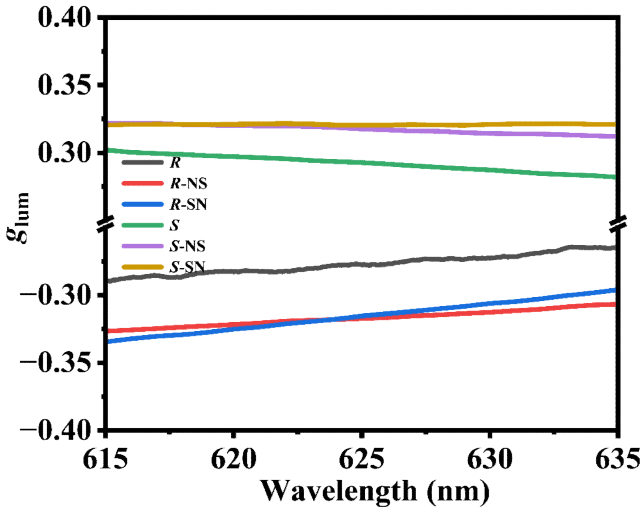

Figure S17. g_{lum} curves of *R/S*-DACAMnBr$_3$ under a 1.6 T magnetic field.

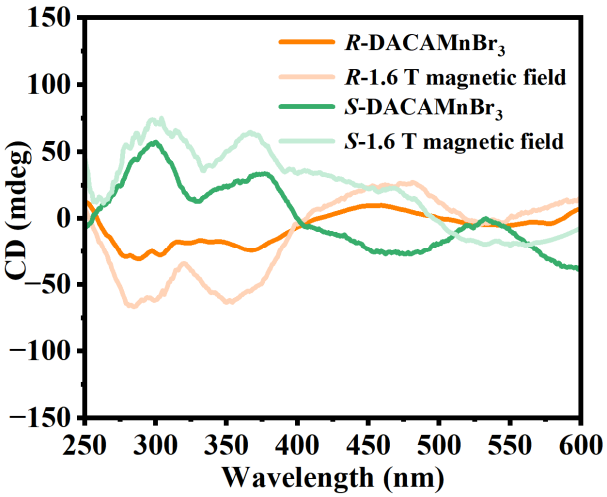

Figure S18. CD curves of *R*-DACAMnBr$_3$ and *S*-DACAMnBr$_3$ with and without magnetic field (1.6 T).

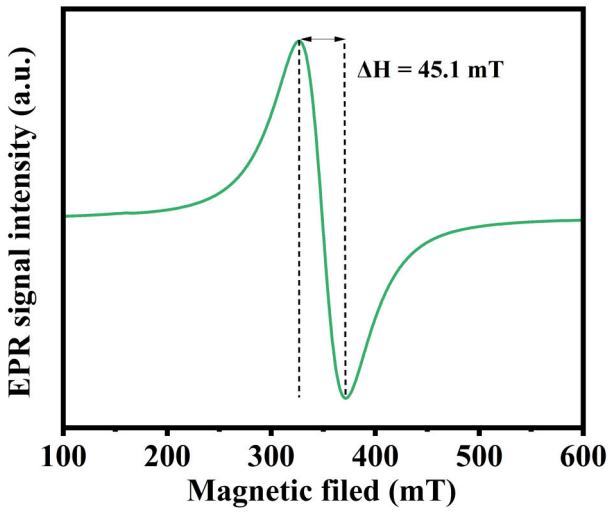

Figure S19. EPR spectrum of *R*-DACAMnBr$_3$ crystals at 298 K.

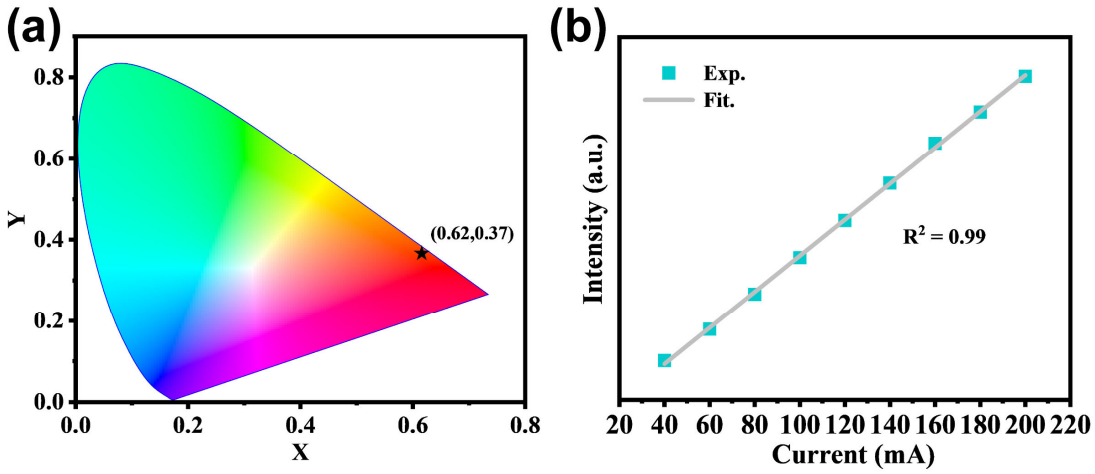

Figure S20. (a) CIE 1931 chromaticity color coordinate of *R*-DACAMnBr$_3$-based CP-LEDs under 365 nm excitation. (b) Emission intensity versus current linear fitting for *R*-DACAMnBr$_3$-based CP-LEDs.

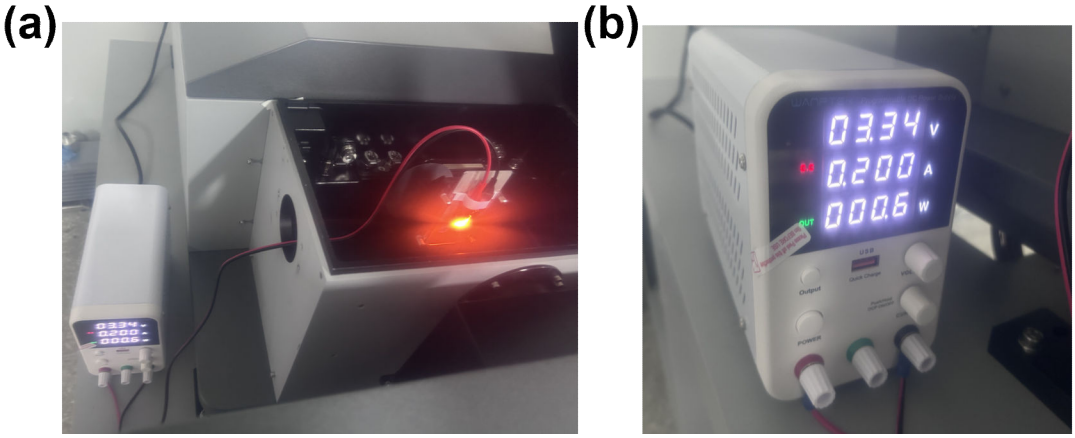

Figure S21. (a) Schematic of the CPL test setup for *R/S*-DACAMnBr$_3$-based CP-LEDs. (b) DC device connection for *R*-DACAMnBr$_3$-based CP-LEDs.

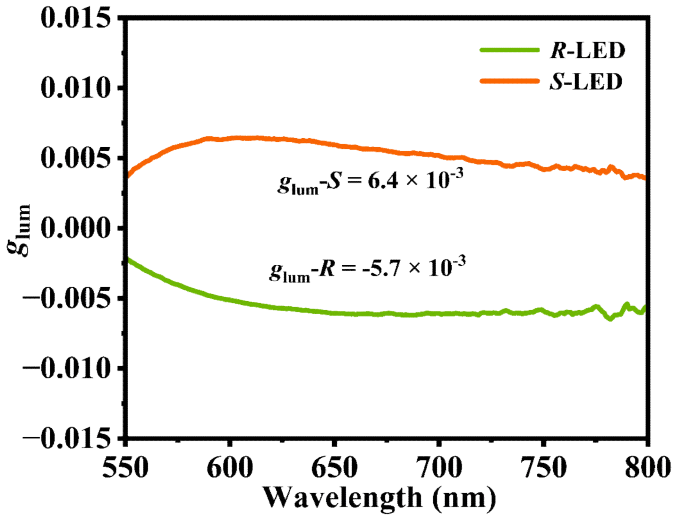

Figure S22. g_{lum} spectra of *R/S*-DACAMnBr$_3$-based CP-LEDs.

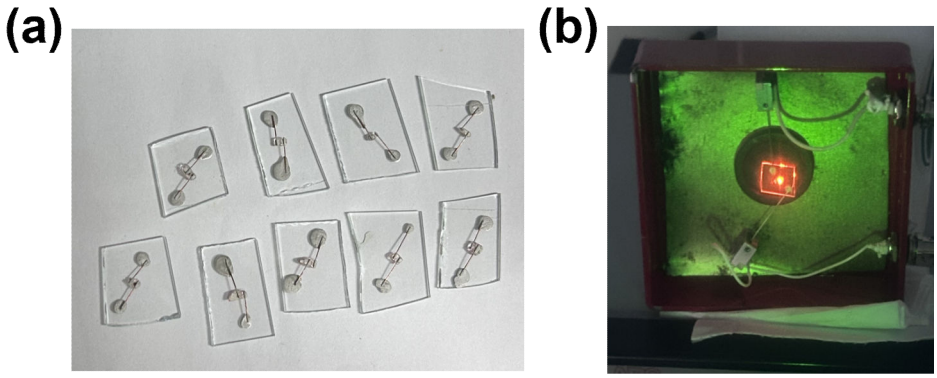

Figure S23. (a) Integrated *R*-DACAMnBr$_3$-based electrodes for photodetectors. (b) Schematic diagram illustrating the operational mechanism of photoelectric detection in practical applications.

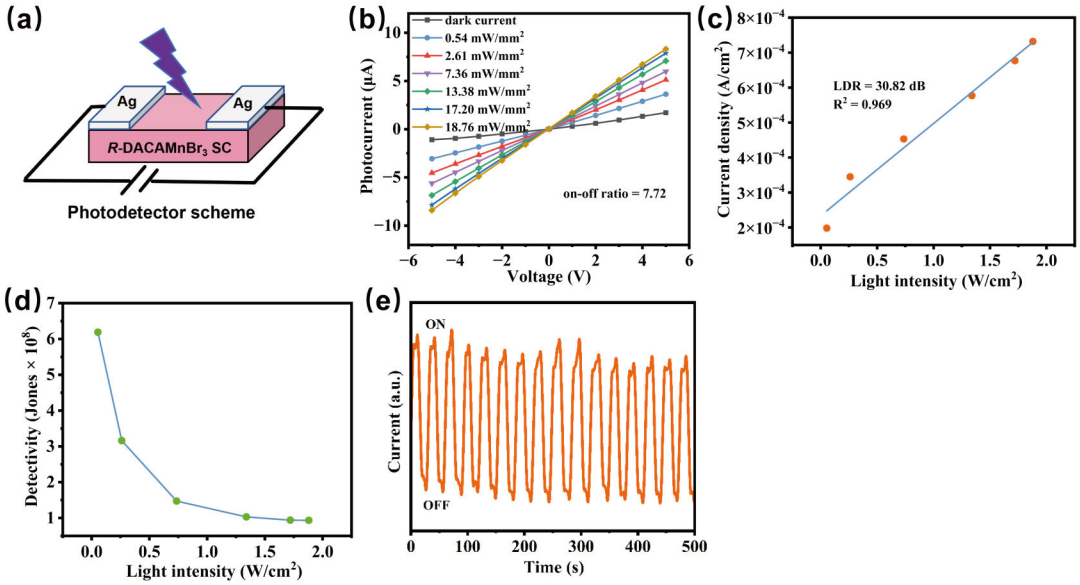

Figure S24. (a) Schematic diagram of the photodetector made by *R*-DACAMnBr$_3$ single crystals. (b) I-V characteristics of the photodetector measured under dark and 266 nm laser illumination. (c) Linear dynamic range, (d) specific detectivity and (e) time-dependent reproducible photocurrent on/off switching of *R*-DACAMnBr$_3$-based photodetector at 266 nm illumination under a 5 V bias.

References

1 K.-L. Wong, J.-C. G. Bunzli and P. A. Tanner, J. Lumin., 2020, **224**, 117256.

2 Y. Wu, S. Wang, Z. Lin, L. Kang, J. Wu, Q. Chen and Z. Lin, *Angew. Chem. Int. Ed.*, 2025, **64**, e202416062.

3 H.-L. Xuan, Y.-F. Sang, L.-J. Xu, D.-S. Zheng, C.-M. Shi and Z.-N. Chen, *Chem. Eur. J.*, 2022, **28**, e202201299.

4 J. Chen, S. Zhang, X. Pan, R. Li, S. Ye, A. K. Cheetham and L. Mao, *Angew. Chem. Int. Ed.*, 2022, **61**, e202205906.

5 J. Li, Q. Luo, J. Wei, L. Zhou, P. Chen, B. Luo, Y. Chen, Q. Pang and J. Z. Zhang, *Angew. Chem. Int. Ed.*, 2024, **63**, e202405310.

6 M. Wang, X. Wang, B. Zhang, F. Li, H. Meng, S. Liu and Q. Zhao, *J. Mater. Chem. C*, 2023, **11**, 3206-3212.

7 M. P. Davydova, L. Meng, M. I. Rakhmanova, I. Y. Bagryanskaya, V. S. Sulyaeva, H. Meng and A. V. Artem'ev, *Adv. Opt. Mater.*, 2023, **11**, 2202811.

8 B. Wang, C. Wang, Y. Chu, H. Zhang, M. Sun, H. Wang, S. Wang and G. Zhao, *J. Alloy. Compd.*, 2022, **910**, 164892.

9 C. Li, Y. Wei, Y. Li, Z. Luo, Y. Liu, M. He, Y. Zhang, X. He, X. Chang and Z. Quan, *Small*, 2024, **20**, 2400338.

10 J.-X. Gao, W.-Y. Zhang, Z.-G. Wu, Y.-X. Zheng and D.-W. Fu, *J. Am. Chem. Soc.*, 2020, **142**, 4756-4761.

11 Y. Asensio, H. B. Jalali, S. Marras, M. Gobbi, F. Casanova, A. Mateo-Alonso, F. Di Stasio, I. Rivilla, L. E. Hueso and B. Martin-Garcia, *Adv. Opt. Mater.*, 2024, **12**, 2400554.

12 X. He, Y. Zheng, Z. Luo, Y. Wei, Y. Liu, C. Xie, C. Li, D. Peng and Z. Quan, *Adv. Mater.*, 2024, **36**, 2309906.

13 T. Zhang, H. Kang, B. Li, J. Zhou, P. Zhao, T. Zhao, X. Li and S. Jiang, *J. Mater. Chem. C*, 2023, **11**, 5461-5468.

14 D.-H. Kong, Y. Wu, C.-M. Shi, H. Zeng, L.-J. Xu and Z.-N. Chen, *Chem. Sci.*, 2024, **15**, 16698-16704.

15 Z. Song, X. Liu, C. Yang, Q. Wu, X. Guo, G. Liu, Y. Wei, L. Meng and Y. Dang, *Adv. Opt. Mater.*, 2024, **12**, 2301272.

16 M. P. P. Davydova, L. Meng, M. I. I. Rakhmanova, Z. Jia, A. S. S. Berezin, I. Y. Bagryanskaya, Q. Lin, H. Meng and A. V. V. Artem'ev, *Adv. Mater.*, 2023, **35**, 2303611.

17 Z. Zhou, T. Jiang, Y. Yang, Y. Deng, M. Wang, Y. Ma, S. Liu and Q. Zhao, *Adv. Opt. Mater.*, 2024, **12**, 2302185.

18 J. Lu, R.-X. Qian, S.-F. Lu, S.-H. Wang, F.-K. Zheng and G.-C. Guo, *Adv. Funct. Mater.*, 2024, **34**, 2410219.